Journal of Alloys and Compounds 515 (2012) 180–185

Contents lists available at SciVerse ScienceDirect

Journal of Alloys and Compounds

journal homepage: www.elsevier.com/locate/jallcom

Solid-state thermal decomposition of the $[Co(NH_3)_5CO_3]NO_3{\cdot}0.5H_2O$ complex: A simple, rapid and low-temperature synthetic route to Co_3O_4 nanoparticles

Saeid Farhadi*, Jalil Safabakhsh

Department of Chemistry, Lorestan University, Khorramabad 68135-465, Iran

ARTICLE INFO

Article history:
Received 6 June 2011
Received in revised form
23 November 2011
Accepted 26 November 2011
Available online 4 December 2011

Keywords:
Co_3O_4 nanoparticles
Pentammine(carbonato)cobalt(III)
Thermal decomposition
Weak ferromagnetic behaviour
p-Type semiconductor

ABSTRACT

Co_3O_4 nanoparticles were easily prepared via the decomposition of the pentammine(carbonato)cobalt(III) nitrate precursor complex $[Co(NH_3)_5CO_3]NO_3{\cdot}0.5H_2O$ at low temperature (175 °C). The product was characterized by thermal analysis, X-ray diffraction (XRD), Fourier-transform infrared spectroscopy (FT-IR), UV–visible spectroscopy, transmission electron microscopy (TEM), energy-dispersive X-ray spectroscopy (EDX), Raman spectroscopy, Brunauer–Emmett–Teller (BET) specific surface area measurements and magnetic measurements. The FT-IR, XRD, Raman and EDX results indicated that the synthesized Co_3O_4 nanoparticles are highly pure and have a single phase. The TEM analysis revealed nearly uniform and quasi-spherical Co_3O_4 nanoparticles with an average particle size of approximately 10 nm. The optical absorption spectrum of the Co_3O_4 nanoparticles showed two direct band gaps of 2.18 and 3.52 eV with a red shift in comparison with previous reported values. The prepared Co_3O_4 nanoparticles showed a weak ferromagnetic behaviour that could be attributed to uncompensated surface spins and/or finite-size effects. Using the present method, Co_3O_4 nanoparticles can be produced without expensive organic solvents and complicated equipment. This simple, rapid, safe and low-cost synthetic route can be extended to the synthesis of other transition-metal oxides.

1. Introduction

Nanoscale transition-metal oxides have received considerable attention because of their interesting size-dependent physical and chemical properties [1–4]. Among these oxides, spinel-type cobalt oxide (Co_3O_4) has been the subject of scientific and technological attention owing to its wide range of applications. This p-type semiconducting material has many applications, e.g., it is used in heterogeneous catalysis, solid-state sensors, pigments, magnetic materials, and electrochromic devices, for energy storage and as anode materials in lithium-ion batteries [5–17]. On the other hand, nanoscale Co_3O_4 structures show interesting magnetic, optical, field emission and electrochemical properties that are not observed by their bulk materials. The prospect of potential applications of Co_3O_4 has led to substantial research and efforts to develop synthetic routes for various types of its nanostructures. In this context, spinel-type Co_3O_4 with different morphologies, such as nanoparticles, hollow nanospheres, nanofibres, nanowires, nanowalls, nanorods, nanotubes, nanoboxes, nanocubes and mesoporous structures, have been described in the literature [18–24]. Among these structures, the preparation of Co_3O_4 nanoparticles has been extensively studied using physical and chemical techniques such as sol–gel method [25], solvothermal method [26,27], combustion method [28], microemulsion [29], chemical spray pyrolysis [30], chemical vapour deposition [31,32], thermal decomposition of cobalt precursors [33–38], ionic liquid-assisted method [39], yeast-assisted biotemplating technique [40], sonochemical method [41], co-precipitation [42], microwave-assisted route [43,44] and mechanochemical method [45]. However, most of these methods utilize toxic and expensive reagents, high temperatures, expensive, complex instruments and long reaction times. Thus, it is desirable to develop a simple, inexpensive and non-toxic route for the preparation Co_3O_4 nanoparticles at a relatively low temperature.

The thermal decomposition of transition-metal complexes is one of the simplest and least expensive techniques for preparing nanosized transition-metal oxides with relatively high specific surface areas at low temperature [46–53]. This technique not only avoided the need for a template and complex apparatus but also exhibited a capacity to control the shape of the target products. By selecting an appropriate precursor coupled with a rational calcination procedure, products with unique sizes and shapes could be obtained. This method also has potential advantages, including operational simplicity, high yield of pure products, absence of solvent, low energy consumption and functional efficiency, exempting the need for special equipment. Therefore, as a continuation of our

* Corresponding author. Tel.: +98 6612202782; fax: +98 6616200088.
E-mail address: sfarhad2001@yahoo.com (S. Farhadi).

0925-8388/$ – see front matter © 2011 Elsevier B.V. All rights reserved.
doi:10.1016/j.jallcom.2011.11.135

previous studies [54–57], we report a rapid and simple thermal decomposition method for the preparation of Co_3O_4 nanoparticles from the pentammine(carbonato)cobalt (III) nitrate complex $[Co(NH_3)_5CO_3]NO_3{\cdot}0.5H_2O$, a new precursor. The product was identified by X-ray diffraction (XRD), Fourier-transform infrared spectroscopy (FT-IR), UV–visible spectroscopy, BET specific surface area measurements, energy-dispersive X-ray spectroscopy (EDX), transmission electron microscopy (TEM), thermal analysis (TGA/DTA) and magnetic measurements. This approach provides a one-step, simple, general and inexpensive method for preparing Co_3O_4 nanocrystals at low temperature (175 °C). Furthermore, to the best of our knowledge, there has been no report on the preparation of spinel-type Co_3O_4 from a classical coordination compound.

2. Experimental

2.1. Preparation of $[Co(NH_3)_5CO_3]NO_3{\cdot}0.5H_2O$ precursor [58]

A solution of 30 g of cobalt(II) nitrate hexahydrate (0.103 mol) in 15 mL of distilled water was thoroughly mixed with a solution of 45 g of ammonium carbonate (0.468 mol) in 45 mL of distilled water and 75 mL of concentrated aqueous ammonium hydroxide (1.11 mol NH_3). Then, 16–20 mL of a 30% H_2O_2 solution was slowly added. After the resulting mixture was cooled in an ice-salt bath overnight, the product was filtered, washed with 50 mL of ice-cold water followed by ethanol and diethyl ether and then dried by drawing air through the filter funnel. This crude material was purified by recrystallization from hot water. The complex was characterized by thermal analysis and FT-IR.

2.2. Preparation of Co_3O_4 nanoparticles

To prepare Co_3O_4 nanoparticles, 2 g of the $[Co(NH_3)_5CO_3]NO_3{\cdot}0.5H_2O$ complex was added to a porcelain crucible and placed in an electric furnace. The complex was heated at the rate of 2 °C min^{-1} from room temperature to 150 °C in air and was maintained at 150 °C for 1 h. Similar experiments were performed with 2 g samples of the complex at the selected temperatures of 175, 200, 250 and 300 °C. The temperatures for calcining the complex were selected from the TGA–DTA data. The decomposition product generated from the complex at each temperature was cooled to room temperature and collected for characterization.

2.3. Characterization techniques

The thermal behaviour of the precursor complex was studied using a Netzsch STA 409 PC/PG thermal analyser at a heating rate of 5 °C min^{-1} in air. Infrared spectra were recorded on a Shimadzu System FT-IR 160 Spectrophotometer using KBr pellets. The XRD patterns were recorded on a Rigaku D-max C III X-ray diffractometer using Ni-filtered Cu Kα radiation (λ = 1.5406 Å) to determine the phases present in the decomposed samples. Raman spectrum was acquired on a Spex 1403 Raman Spectrometer. Optical absorption spectrum was recorded on a Shimadzu 1650PC UV–vis spectrophotometer in the 250–700 nm wavelength range at room temperature. The samples for UV–vis studies were well dispersed in distilled water by sonication for 25 min to form a homogeneous suspension. Particle sizes were determined by a transmission electron microscope (TEM, Philips CM10) equipped with a link energy-dispersive X-ray (EDX) analyser. The powders were ultrasonicated in ethanol and a drop of the suspension was dried on a carbon-coated microgrid for TEM measurements. The specific surface area of the product was measured by the BET method using an N_2 adsorption–desorption isotherm carried out at −196 °C on a surface area analyser (Micromeritics ASAP 2010). Before each measurement, the sample was degassed at 150 °C for 2 h. Magnetic measurements were carried out at room temperature using a vibrating sample magnetometer (Meghnatis Daghigh Kavir Co.) with a maximum magnetic field of 10 kOe.

3. Results and discussion

Initially, the thermal behaviour of the $[Co(NH_3)_5CO_3]NO_3{\cdot}0.5H_2O$ complex was studied by thermal analysis. Fig. 1 shows TGA/DTA curves recorded at a constant heating rate of 5 °C min^{-1} in the 25–300 °C temperature range. The TGA curve in Fig. 1(a) shows that the decomposition of the complex occurs in three main stages. The first stage occurs at 105 °C and shows a 3.25% weight loss, which can be related to the liberation of half a mole of H_2O per mole of the complex. The second stage occurs at approximately 145–150 °C and shows a 22.5% weight loss, which is consistent with the theoretical value of 22.37% caused by the loss of one mole of NH3 and one mole of CO_2 per mole of the complex. On further heating, the third stage occurs in which an extensive weight loss (43.25%) is observed in the 150–175 °C range, which is accompanied by an explosive decomposition of the residue complex. Above 175 °C, the weight remains constant, confirming the complete decomposition of the complex. The combined weight loss from all stages is approximately 69%, which is consistent with the theoretical value (69.2%) that is calculated for the formation of Co_3O_4 from the complex. The DTA curve of the $[Co(NH_3)_5CO_3]NO_3{\cdot}0.5H_2O$ complex in Fig. 1(b) shows characteristic endothermic and exothermic peaks, consistent with the TGA data. The small endothermic peaks at 105 °C can be explained by the loss of half a mole of H_2O. The broad endothermic peak at 145–150 °C can be attributed to the loss of one mole of NH_3 and the decomposition of an unstable monodentate carbonate ligand (dissociation of the Co—OCO_2 bond). The decomposition of the residue complex shows a small endothermic peak at 170 °C, which is immediately followed by a large exothermic peak near 175 °C. This sharp exothermic peak can be explained by the explosive decomposition of the complex via an intramolecular redox process occurring between the reductant (NH_3 ligands) and the oxidant (NO_3^-). The explosive reaction resulted in the formation of solid

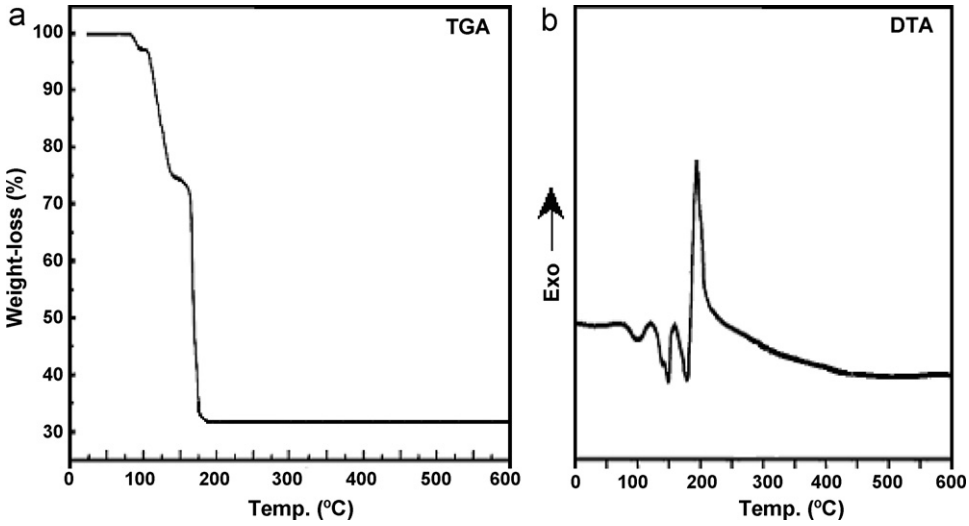

Fig. 1. (a) TGA and (b) DTA curves of the $[Co(NH_3)_5CO_3]NO_3{\cdot}0.5H_2O$ complex.

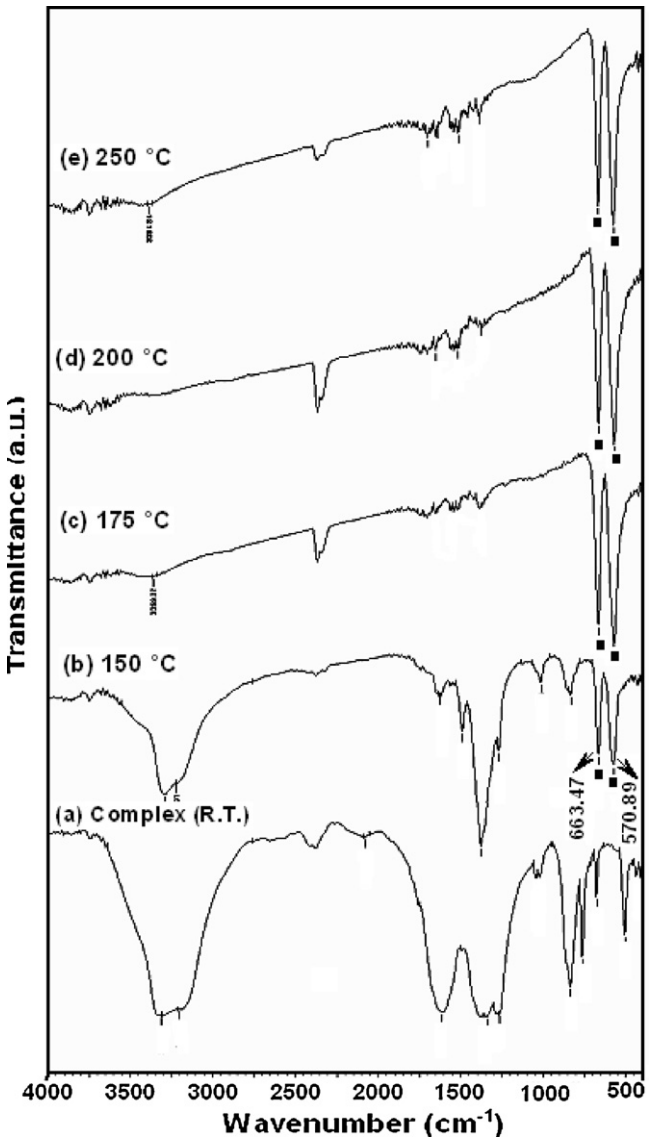

Fig. 2. FT-IR spectra of the $[Co(NH_3)_5CO_3]NO_3{\cdot}0.5H_2O$ complex decomposed at various temperatures; ■: Co_3O_4 phase.

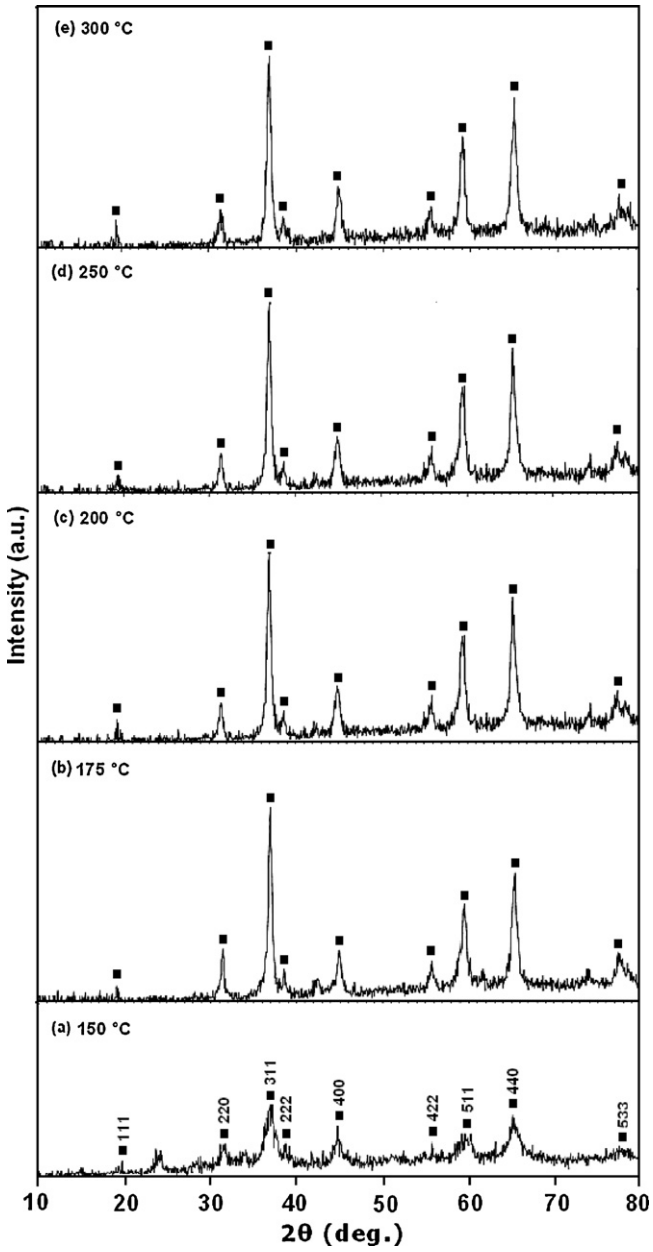

Fig. 3. XRD patterns of the $[Co(NH_3)_5CO_3]NO_3{\cdot}0.5H_2O$ complex decomposed at selected temperatures; ■: Co_3O_4 phase.

Co_3O_4 and gaseous products (i.e., NH_3, N_2, NO or N_2O and H_2O), according to the following reaction:

$$3[Co(NH_3)_5CO_3]NO_3{\cdot}0.5H_2O \rightarrow Co_3O_4 + 10NH_3 + 8H_2O + 3CO_2 + 0.5NO + 3.75N_2$$

Fig. 2 shows the FT-IR spectra of the $[Co(NH_3)_5CO_3]NO_3{\cdot}0.5H_2O$ complex and its decomposition products at different temperatures. For the complex (Fig. 2(a)), the characteristic stretching bands of NH_3, CO_3 and NO_3 are observed at approximately 3500–3000, 1600 and 1350 cm^{-1}, respectively [59]. As shown in Fig. 2(b), the intensity of these bands decreases when the complex is heated at 150 °C. At this temperature, two small absorption bands (■) that are assigned to the Co—O stretching bands of Co_3O_4 appear at approximately 663.47 and 570.89 cm^{-1}, respectively, providing clear evidence for the presence of crystalline Co_3O_4 [60]. This observation confirms that the formation of Co_3O_4 nanocrystals begins at approximately 150 °C. As can be clearly seen in Fig. 2(c), all bands of the complex disappear as the temperature increases to 175 °C, consistent with the TGA–DTA data described above, and only two characteristic strong bands of the spinel-type Co_3O_4 structure are observed [60]. As shown in Fig. 2(d and e), FT-IR spectra of the samples that were decomposed in the 200–250 °C range show only the strong bands associated with Co_3O_4 without obvious changes. It is noted that a tiny band at approximately 2360 cm^{-1} in the spectrum of some samples is associated with the presence of atmospheric CO_2 [61].

XRD patterns of the decomposition products of the $[Co(NH_3)_5CO_3]NO_3{\cdot}0.5H_2O$ complex at various temperatures are shown in Fig. 3. Fig. 3(a) shows the XRD pattern of the complex heated at 150 °C. The XRD pattern of the decomposed sample at this temperature reveals broad and weak diffraction peaks with 2θ values at 19.50°, 31.37°, 37.02°, 39.10°, 44.97°, 55.84°, 59.58°, 65.46° and 77.62° that are assigned to the crystal planes of (1 1 1), (2 2 0), (3 1 1), (2 2 2), (4 0 0), (4 2 2), (5 1 1), (4 4 0) and (5 3 3) of crystalline Co_3O_4, respectively, consistent with the literature values (JCPDS Card No. 76-1802). This result confirms that the formation of the Co_3O_4 phase started at 150 °C. As shown in Fig. 3(b), the intensity of the characteristic peaks of the Co_3O_4 phase increases considerably as the temperature increases to

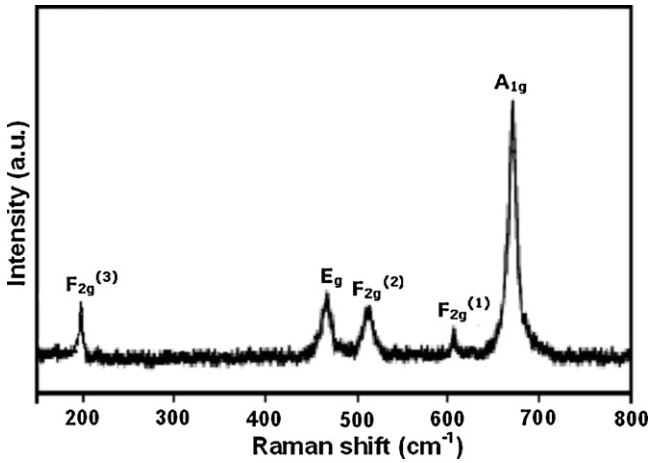

Fig. 4. Raman spectrum of the Co_3O_4 nanoparticles.

175 °C. At this temperature, complete decomposition of the complex is observed, which is in good agreement with the TGA–DTA and FT-IR results. No characteristic peaks of impurity phases such as CoO and CoOOH are present, indicating that the final product is highly pure. The considerable broadening of the diffraction peaks demonstrates the nanometre nature of the Co_3O_4 particles. The average crystallite size of the Co_3O_4 powder prepared at 175 °C is approximately 11 nm as determined from the XRD pattern parameters according to the classical Debye–Scherrer equation [62], $D_{XRD} = 0.9\lambda/(\beta \cos\theta)$, where D_{XRD} is the average crystallite size, λ is the wavelength of $Cu_{K\alpha}$, β is the full width at half maximum of the diffraction peak and θ is the Bragg angle. As seen in Fig. 3(c–e), the width of the Co_3O_4 peaks decreases as the decomposition temperature increases to 200, 250 and then 300 °C because of crystallite growth, but no new phase is observed.

The Raman spectrum of the Co_3O_4 nanoparticles shown in Fig. 4 displays five bands ($A_{1g} + E_g + 3F_{2g}$) in the 150–800 cm^{-1} range. The band at 670 cm^{-1} with A_{1g} symmetry is attributed to the octahedral CoO_6 sites of the crystalline Co_3O_4 phase and is in agreement with the literature value [63]. The bands with medium intensity located at approximately 470 and 510 cm^{-1} have the E_g and $F_{2g}^{(2)}$ symmetry, respectively, whereas the weak band located at 606 cm^{-1} has the $F_{2g}^{(1)}$ symmetry. The band at approximately 191 cm^{-1} is attributed to the $F_{2g}^{(3)}$ mode of the tetrahedral CoO_4 sites [64]. This result further confirms the formation of the Co_3O_4 nanocrystals. No vibrational modes due to impurities are observed. Furthermore, the peak positions of the five active modes shift to low wavenumbers (ca. 10–20 cm^{-1}) in comparison with those of the bulk Co_3O_4 sample [65]. This phenomenon is attributed to the optical phonon confinement effect in nanostructures that can cause uncertainty in the phonon wave vectors and a consequential downshift of the Raman peaks [66].

The size and shape of the Co_3O_4 particles prepared by the thermal decomposition of the $[Co(NH_3)_5CO_3]NO_3{\cdot}0.5H_2O$ complex at 175 °C were investigated by TEM. The TEM analysis reveals very fine, loosely aggregated particles. The particles have uniform size and a homogeneous sphere-like morphology with a narrow size distribution. As shown in the inset in Fig. 5, the Co_3O_4 nanoparticles exhibit a narrow size distribution (6–14 nm) and the mean diameter of the particles is approximately 10 nm, which resembles the average particle size calculated from the XRD data. From the TEM image, it was concluded that this preparation method successfully overcame the problem of agglomeration and is appropriate for the production of small-sized Co_3O_4 nanoparticles.

The EDX spectrum of the product is shown in Fig. 6. The EDX analysis of the Co_3O_4 nanoparticles confirms that the sample

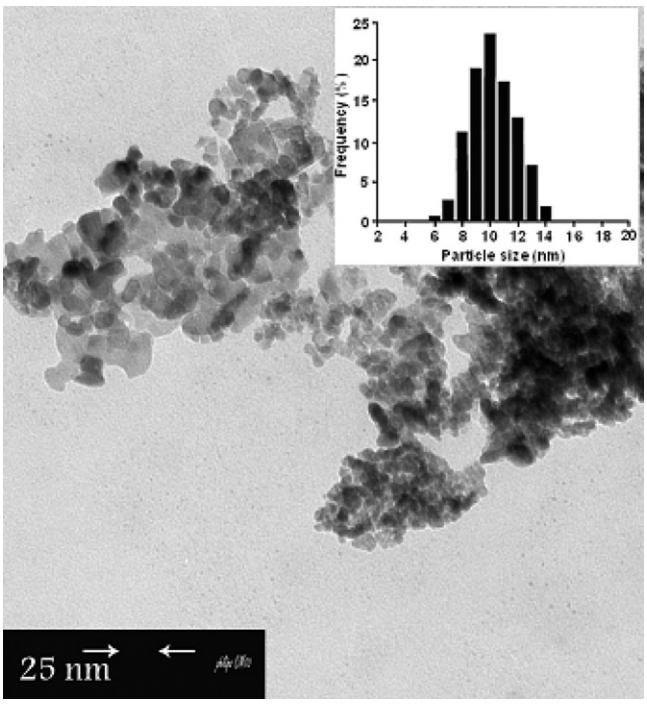

Fig. 5. TEM image of the Co_3O_4 nanoparticles.

contains only Co and O. The Al and Au signals originate from the Al base and the Au sprayed during sample preparation, respectively. The experimental atomic percentages of Co and O are found to be 43.18% and 56.82%, respectively. The atomic ratio of Co to O is approximately 3:3.96, which further confirms that the final product is composed of only Co_3O_4 nanocrystals.

BET surface area measurements were also conducted using the Co_3O_4 nanoparticles obtained from the decomposition of the complex at 175 °C. The specific surface area of the sample is 85.50 m^2/g. Assuming that the Co_3O_4 nanoparticles are almost spherical, as confirmed by TEM, the surface area can be used to estimate the particle size according to the equation $D_{BET} = 6000/(\rho \times S_{BET})$, where D_{BET} is the diameter of a spherical particle (in nm), ρ is the theoretical density of Co_3O_4 (6.08 g/cm^3) and S_{BET} is the specific surface area of the Co_3O_4 powder in m^2/g. The particle size calculated from the surface area data is approximately 11.5 nm, which is in good agreement with the XRD and TEM results.

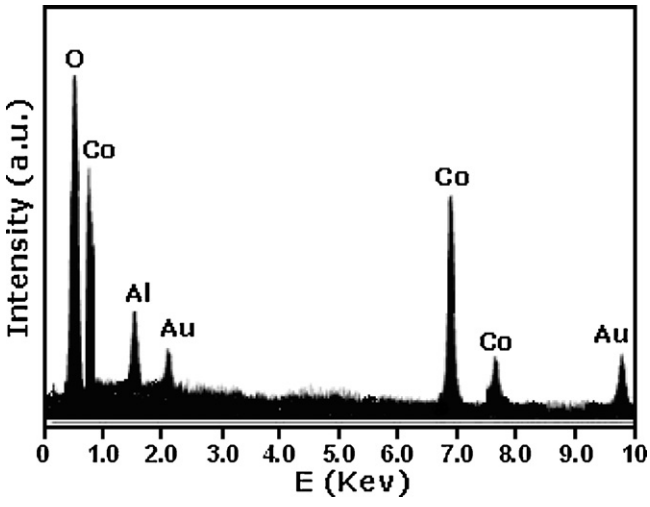

Fig. 6. EDX spectrum of the Co_3O_4 nanoparticles.

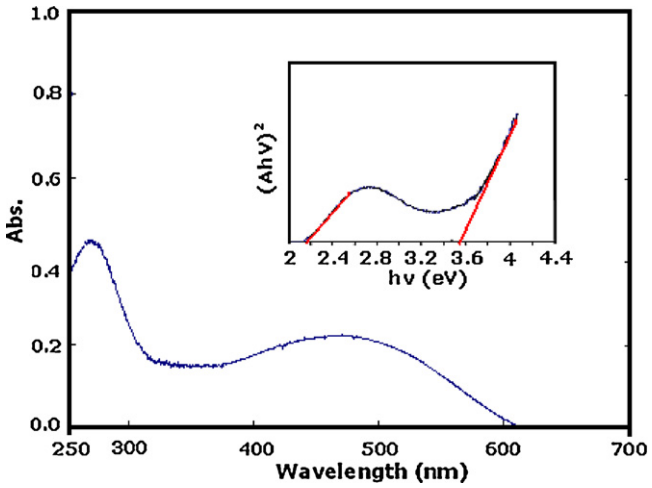

Fig. 7. UV–vis spectrum and $(Ah\nu)^2$–$h\nu$ curve (inset) of the Co_3O_4 nanoparticles.

The optical properties of the Co_3O_4 nanoparticles were investigated at room temperature by UV–vis spectroscopy. Fig. 7 shows the absorbance spectrum of the Co_3O_4 sample with two absorption bands in 200–350 and 400–580 nm wavelength ranges. The first band can be assigned to the $O^{2-} \rightarrow Co^{2+}$ charge-transfer process while and the second one to the $O^{2-} \rightarrow Co^{3+}$ charge transfer [67]. Co_3O_4 is a p-type semiconductor, and the absorption band gap (E_g) can be determined by the following equation [68]: $(Ah\nu)^2 = K(h\nu - E_g)$, where $h\nu$ is the photon energy (eV), A is the absorption coefficient, K is a constant and E_g is the band gap. The band gap can be estimated by extrapolating the linear region in the plot of $(Ah\nu)^2$ versus photon energy. As shown in the inset in Fig. 7, two absorption peaks yield two E_g values for the sample. The empirical E_g values of the Co_3O_4 nanoparticles prepared in this study are 2.18 and 3.52 eV, which are greater than the bulk values (1.77 and 3.37 eV, respectively) [40,69]. This suggests that the Co_3O_4 nanocrystals synthesized via the present method are well within the quantum confinement regime which allows fine tuning of their material properties. Our results are generally consistent with the reported data for Co_3O_4 nanoparticles [69]. These findings confirmed that the optical band gap energies increase as the crystallite size decreases.

Room-temperature magnetic measurements of the Co_3O_4 nanoparticles prepared at 175 and 200 °C are shown in Fig. 8. As shown in the inset in Fig. 8(a and b), the thin hysteresis loop

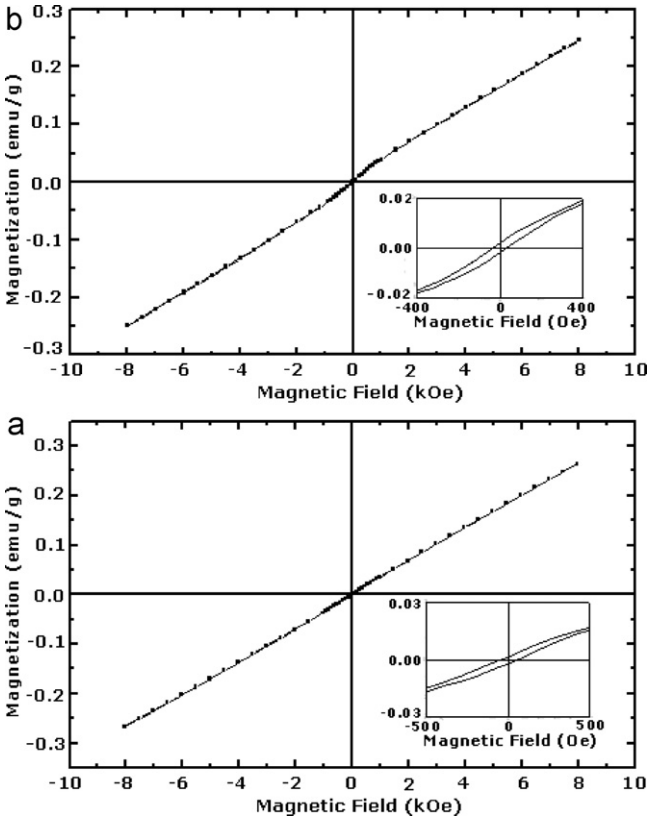

Fig. 8. Room-temperature magnetization curves as a function of applied magnetic field for the Co_3O_4 nanoparticles prepared at: (a) 175 °C and (b) 200 °C. The insets show the magnetization of the hysteresis loop.

is characteristic of weak ferromagnetic behaviour, although bulk Co_3O_4 is antiferromagnetic [70]. From the insets, the coercive field and the remanent magnetization are estimated to be less than 50 Oe and 0.002 emu/g, respectively. The low coercive field and remanent magnetization confirm that the Co_3O_4 nanoparticles exhibit a weak ferromagnetic behaviour. The maximum field applied (8 kOe) does not saturate the magnetization, and the magnetization at this applied field is approximately 0.25 emu/g. The ferromagnetic behaviour of the nanoparticles can be explained as follows: bulk Co_3O_4 has a normal spinel structure with antiferromagnetic exchange between ions that occupy the tetrahedral and

Table 1
Comparison of the results obtained for the preparation of Co_3O_4 nanoparticles in the present work with some reported methods.

Entry	Preparation method	Conditions (solvent, and surfactants)	Temperature (°C)	Time (h)	Particle size (nm)	Particle size distribution (nm)	Ref.
1	Sol–gel method	Liquid N_2, Propionic acid	260	2	300	200–400	[25]
2	Hydrothermal method	Water, PVP[a]	150	16	350	300–500	[26]
3	Combustion method	Water, PVA[b]	400	2	33	–	[28]
4	Microemulsion method	Water/cyclohexane/n-pentanol, CTAB[c]	450	3	–	80–150	[29]
5	Ionic-liquid assisted method	[BMIM]OH[d]	RT	6	30	10–50	[39]
6	Sonochemical method	Water/NaOH, TMAH[e]	Ultrasonic irradiation	1	45	20–60	[41]
7	Microwave method	Ethylene glycol, TOPO[f]	400	3	6	4–8	[44]
8	Mechanochemical method	–	300	2	13	–	[45]
9	Thermal treatment process	–	500	5	30	30–50	[52]
10	Thermal decomposition	–	175	1	10	6–14	This work

[a] PVP: polyvinylpyrrolidone.
[b] PVA: polyvinyl alcohol.
[c] CTAB: cetyltrimethylammonium bromide.
[d] [BMIM]OH: 1-n-butyl-3-methylimidazolium hydroxide (an ionic liquid).
[e] TMAH: tetramethylammonium hydroxide.
[f] TOPO: trioctyl phosphine oxide.

octahedral sites [70]. It has zero net magnetization owing to the complete compensation of sublattice magnetization. Hence, the change from an antiferromagnetic state for bulk Co_3O_4 to a weak ferromagnetic state for Co_3O_4 nanoparticles can be ascribed to the uncompensated surface spins and/or finite-size effects [36,71,72]. It is well known that the magnetic properties of nanomaterials are strongly dependent on the shape and size of their particles, crystallinity, magnetization direction and so on.

To elucidate the advantages of the present method, we have compared the empirical results with some reported studies in Table 1. From Table 1, it is clear that the present method is more suitable and/or superior to other methods with respect to the reaction conditions, reaction temperature, reaction time, average particle size and particle size distribution. It can be seen that most of these methods are associated with one or more disadvantages, such as prolonged reaction times, harsh reaction conditions, high-temperature requirement, use of harmful organic solvents, use of expensive solvents and surfactants and the formation of particles with very large sizes and wide size distribution. Using the present method, Co_3O_4 nanoparticles can be produced at low temperature in the absence of solvent, surfactant and any expensive, complicated equipment.

4. Conclusions

In summary, pure nanosized Co_3O_4 particles with an average particle size of 10 nm were successfully synthesized by the thermal decomposition of the $[Co(NH_3)_5CO_3]NO_3{\cdot}0.5H_2O$ complex as a new precursor in the 150–200 °C range. From this complex, Co_3O_4 nanoparticles are formed via the dehydration and subsequent explosive redox reaction between the NH_3 ligands as the reducing agent and the NO_3^- ions as the oxidizing agent. By this method, uniform and sphere-like Co_3O_4 nanoparticles with weak agglomeration, narrow size distribution and weak ferromagnetic behaviour can be obtained. The optical absorption band gaps of the Co_3O_4 nanoparticles were estimated to be approximately 2.18 and 3.52 eV, which are red shifted in comparison with previously reported values. This method is simple, inexpensive, safe and suitable for the industrial production of high-purity Co_3O_4 nanoparticles for various applications. Furthermore, the method may be advantageous for the synthesis of other metal oxide nanostructures.

Acknowledgements

The authors gratefully acknowledge the Lorestan University Research Council and Iran Nanotechnology Initiative Council (INIC) for their financial support.

References

[1] Y.-Q. Kang, M.-S. Cao, J. Yuan, L. Zhang, B. Wen, X.-Y. Fang, J. Alloys Compd. 495 (2010) 254–259.
[2] Y.-Q. Kang, M.-S. Cao, J. Yuan, X.-L. Shi, Mater. Lett. 63 (2009) 1344–1346.
[3] X.-L. Shi, M.-S. Cao, X.-Y. Fang, J. Yuan, Y.-Q. Kang, W.-L. Song, Appl. Phys. Lett. 93 (2008) 223112–223114.
[4] X.-L. Shi, M.-S. Cao, J. Yuan, X.-Y. Fang, Appl. Phys. Lett. 95 (2009) 163108–163110.
[5] M. Casas-Cabanas, G. Binotto, D. Larcher, A. Lecup, V. Giordani, J.M. Tarascon, Chem. Mater. 21 (2009) 1939–1947.
[6] W.-Y. Li, L.-N. Xu, J. Chen, Adv. Funct. Mater. 15 (2005) 851–857.
[7] S.-L. Chou, J.-Z. Wang, H.-K. Liu, S.-X. Dou, J. Power Sources 182 (2008) 359.
[8] E.M. Logothesis, K. Park, A.H. Meitzler, K.R. Laud, Appl. Phys. Lett. (1975) 209–211.
[9] T. Maruyama, S. Arai, J. Electrochem. Soc. 143 (1996) 1383–1386.
[10] E. Antolini, Mater. Res. Bull. 32 (1997) 9–14.
[11] Y.G. Li, B. Tan, Y.Y. Wu, Nano Lett. 8 (2008) 265–270.
[12] X.W. Lou, D. Deng, J.Y. Lee, L.A. Archer, Adv. Mater. 20 (2008) 258–262.
[13] P. Poizot, S. Laruelle, S. Grugeon, L. Dupont, J.M. Tarascon, Nature 407 (2000) 496–499.
[14] K. Ramachandram, C.O. Oriakhi, M.M. Lerner, V.R. Koch, Mater. Res. Bull. 31 (1996) 767–772.
[15] S. Noguchi, M. Mizuhashi, Thin Solid Films 77 (1981) 99–106.
[16] T. Sugimoto, E. Matijevic, J. Inorg. Nucl. Chem. 41 (1979) 165–172.
[17] S.A. Makhlouf, J. Magn. Mater. 246 (2002) 184–190.
[18] T. Li, S.G. Yang, L.S. Huang, B.X. Gu, Y.W. Du, Nanotechnology 15 (2004) 1479–1482.
[19] B.B. Lakshmi, C.J. Patrissi, C.R. Martin, Chem. Mater. 9 (1997) 2544–2550.
[20] G.X. Wang, X.P. Shen, J. Horvat, B. Wang, H. Liu, D. Wexler, J. Yao, J. Phys. Chem. C 113 (2009) 4357–4361.
[21] N. Du, H. Zhang, B.D. Chen, J.B. Wu, X.Y. Ma, Z.H. Liu, Y.Q. Zhang, D.R. Yang, X.H. Huang, J.P. Tu, Adv. Mater. 19 (2007) 4505–4509.
[22] L.H. Zhuo, J.C. Ge, L.H. Cao, B. Tang, Cryst. Growth Des. 9 (2009) 1–6.
[23] T. He, D.R. Chen, X.L. Jiao, Y.L. Wang, Adv. Mater. 18 (2006) 1078–1082.
[24] A. Rumplecker, F. Kleitz, E.L. Salabas, F. Schuth, Chem. Mater. 19 (2007) 485–496.
[25] M.E. Baydi, G. Poillerat, J.L. Rehspringer, J.L. Gautier, J.F. Koenig, P. Chartier, J. Solid State Chem. 109 (1994) 281–288.
[26] J. Ma, S. Zhang, W. Liu, Y. Zhao, J. Alloys Compd. 490 (2010) 647–651.
[27] L. Li, Y. Chu, Y. Liu, J.L. Song, D. Wang, X.W. Du, Mater. Lett. 62 (2008) 1507–1510.
[28] W. Wen, J.-M. Wu, J.-P. Tu, J. Alloys Compd. (2011), doi:10.1016/j.jallcom.2011.11.019.
[29] R. Xu, J. Wang, Q. Li, nG. Sun, E. Wang, S. Li, J. Gu, M. Ju, J. Solid State Chem. 182 (2009) 3177–3182.
[30] D.Y. Kim, S.H. Ju, H.Y. Koo, S.K. Hong, Y.C. Kangf, J. Alloys Compd. 417 (2006) 254–258.
[31] A.U. Mane, K. Shalini, A. Wohlfart, A. Devi, S.A. Shivashankar, J. Cryst. Growth 240 (2002) 157–163.
[32] Y. Xuan, R. Liu, Y.Q. Jia, Mater. Chem. Phys. 53 (1998) 256–261.
[33] A. Rumplecker, F. Kleitz, E.L. Salabas, F. Schüth, Chem. Mater. 19 (2007) 485–496.
[34] W.W. Wang, Y.J. Zhu, Mater. Res. Bull. 40 (2005) 1929–1935.
[35] L.X. Yang, Y.J. Zhu, L. Li, L. Zhang, H. Tong, W.W. Wang, Eur. J. Inorg. Chem. (2006) 4787–4792.
[36] F. Mohandes, F. Davar, M. Salavati-Niasari, J. Magn. Magn. Mater. 322 (2010) 872–877.
[37] J. Jiang, L. Li, Mater. Lett. 61 (2007) 4894–4896.
[38] L. Ren, P. Wang, Y. Han, C. Hu, B. Wei, Mater. Phys. Lett. 476 (2009) 78–83.
[39] D. Zou, C. Xu, H. Luo, L. Wang, T. Ying, Mater. Lett. 62 (2008) 1976–1978.
[40] L. Yang, W. Guan, B. Bai, Q. Xu, Y. Xiang, J. Alloys Compd. 504 (2010) L10–L13.
[41] A. Askarinejad, Ali Morsali, Ultrason. Sonochem. 16 (2009) 124–131.
[42] T. Lai, Y. Lai, C. Lee, Y. Shu, C. Wang, Catal. Today 131 (2008) 105–110.
[43] C. Sun, X. Su, F. Xiao, C. Niu, J. Wang, Sens. Actuators B: Chem. 157 (2011) 681–685.
[44] A.S. Bhatt, D.K. Bhat, C.-W. Tai, M.S. Santosh, Mater. Chem. Phys. 125 (2011) 347–350.
[45] H. Yang, Y. Hu, X. Zhang, G. Qiu, Mater. Lett. 58 (2004) 387–389.
[46] A. Pathak, S. Mohapatra, S. Mohapatra, S.S.K. Biswas, D. Dhak, N.K. Pramanik, A. Tarafdar, P. Pramanik, Am. Ceram. Soc. Bull. 83 (2004) 9301–9306.
[47] M. Salavati-Niasari, F. Davar, M. Mazaheri, Mater. Lett. 62 (2008) 1890–1892.
[48] M. Salavati-Niasari, F. Davar, Mater. Lett. 63 (2009) 441–443.
[49] M. Salavati-Niasari, F. Davar, M. Mazaheri, J. Alloys Compd. 470 (2009) 502–506.
[50] F. Davar, Z. Fereshteh, M. Salavati-Niasari, J. Alloys Compd. 476 (2009) 797–801.
[51] M. Salavati-Niasari, Z. Fereshteh, F. Davar, Polyhedron 28 (2009) 1065–1068.
[52] M. Khansari, A. Salavati-Niasari, F. Davar, Inorg. Chim. Acta 362 (2009) 4937–4942.
[53] M. Salavati-Niasari, N. Mir, F. Davar, J. Phys. Chem. Solids 70 (2009) 847–852.
[54] S. Farhadi, N. Rashidi, Polyhedron 29 (2010) 2959–2965.
[55] S. Farhadi, Z. Roostaei-Zaniyani, Polyhedron 30 (2011) 1244–1249.
[56] S. Farhadi, Z. Roostaei-Zaniyani, Polyhedron 30 (2011) 971–975.
[57] S. Farhadi, M. Kazem, F. Siadatnasab, Polyhedron 30 (2011) 606–613.
[58] F. Basolo, R.K. Murmann, Inorg. Synth. 4 (1953) 171.
[59] K. Nakamoto, Infrared and Raman Spectra of Inorganic and Coordination Compounds, Part B: Applications in Coordination, Organometallic, and Bioinorganic Chemistry, sixth ed., Wiley, New York, 2009.
[60] B. Pejova, A. Isahi, M. Najdoski, Mater. Res. Bull. 36 (2001) 161–170.
[61] H.Y. Guan, C.L. Shao, S.B. Wen, Mater. Chem. Phys. 82 (2003) 1002–1006.
[62] H.P. Klug, L.E. Alexander, X-ray Diffraction Procedures, second ed., Wiley, New York, 1964.
[63] Z.V. Marinkovic Stanojevic, N. Romcevic, B. Stojanovic, J. Eur. Ceram. Soc. 27 (2007) 903–908.
[64] C.V. Ramana, M. Massot, C.M. Julien, Surf. Interface Anal. 37 (2005) 412–416.
[65] V.G. Hadjiev, M.N. Iliev, I.V. Vergilov, J. Phys. C: Solid State Phys. 21 (1988), L199-L104.
[66] B. Cao, W. Cai, G. Duan, Y. Li, Q. Zhao, D. Yu, Nanotechnology 16 (2005) 2567–2571.
[67] T. He, D.R. Chen, X.L. Jiao, Y.L. Wang, Y.Z. Duan, Chem. Mater. 17 (2005) 4023–4030.
[68] A. Gulino, P. Dapporto, P. Rossi, I. Fragala, Chem. Mater. 15 (2003) 3748–3752.
[69] F. Gu, C. Li, Y. Hu, L. Zhang, J. Cryst. Growth 304 (2007) 369–373.
[70] Y. Ichiyanagi, Y. Kimishima, S. Yamada, J. Magn. Magn. Mater. 272–276 (2004) e1245–e1246.
[71] R.H. Kodama, S.A. Makhlouf, A.E. Berkowitz, Phys. Rev. Lett. 79 (1997) 1393–1396.
[72] T. Ozkaya, A. Baykal, M.S. Toprak, Y. Koseoglu, Z. Durmus, J. Magn. Magn. Mater. 321 (2009) 2145–2149.